Supplementary Information (SI) for EES Catalysis.
This journal is © The Royal Society of Chemistry 2025

Supplementary Materials for

Elevated Temperature and Pressure Drive Ampere-Level CO_2 electroreduction to CO in a Membrane Electrode Assembly Electrolyzer

Yang Li[1], Huiyue Liu[1], Raj Jithu[1], Mohammad Pishnamazi[1], Jingjie Wu[1*]

[1]Department of Chemical and Environmental Engineering, University of Cincinnati, Cincinnati, OH 45221, USA

*Correspondence: jingjie.wu@uc.edu (J. Wu)

This file includes:

Supplementary
Figure S1 to S20

Techno-economic analysis

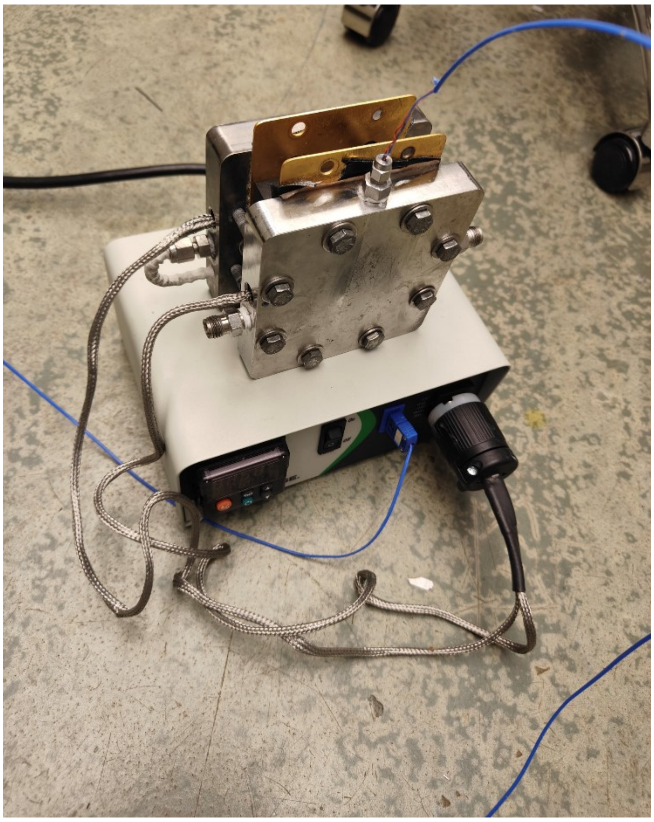

Figure S1. Photos of the MEA cell and the PID Temperature Controller.

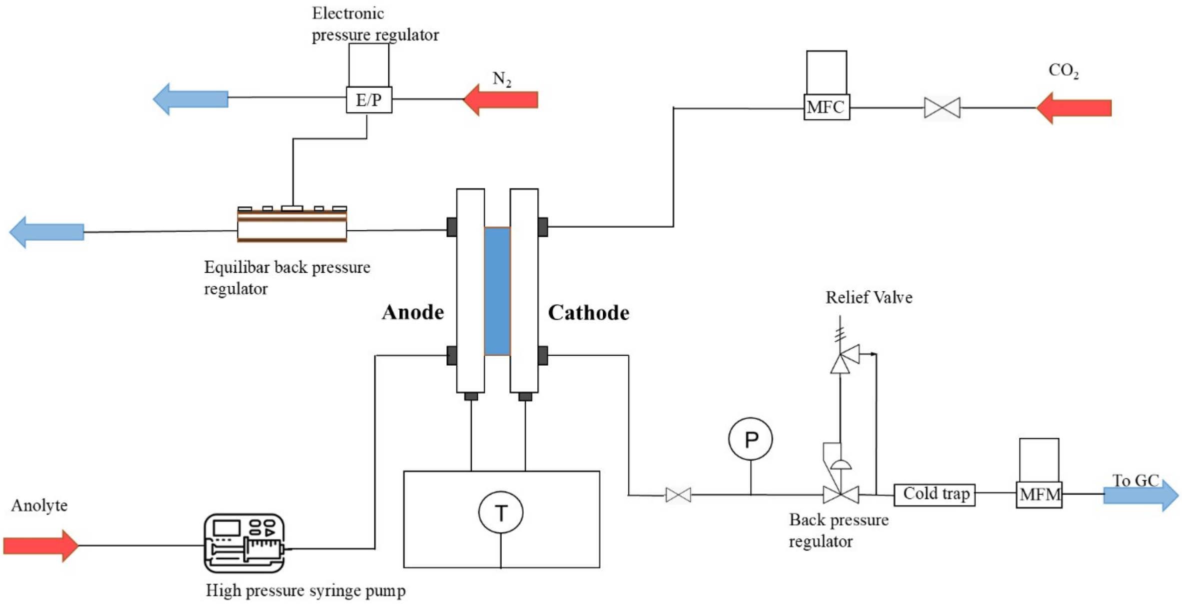

Figure S2. Schematic of the setup for pressurized experiments.

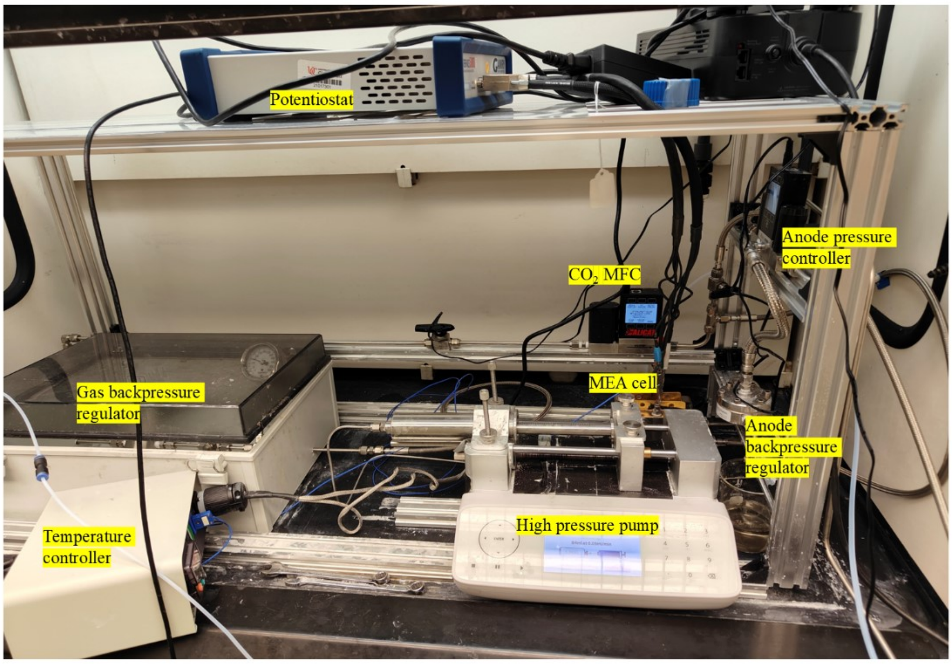

Figure S3. Photograph of the complete experimental setup for the pressurized CO_2 electrolyzer.

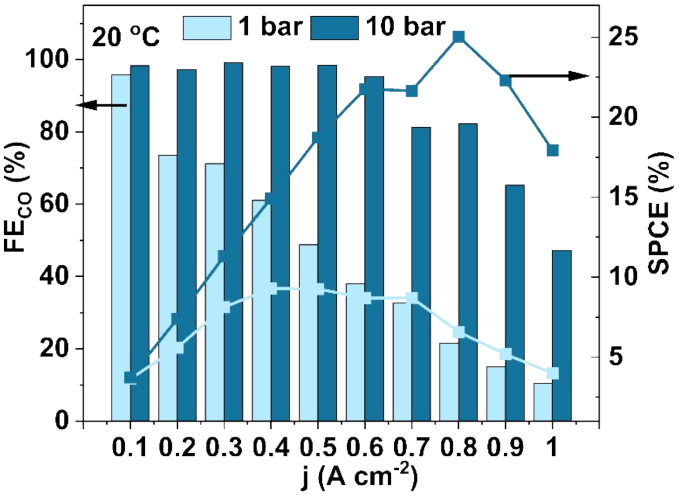

Figure S4. FE$_{CO}$ and single-pass CO_2 conversion efficiency (SPCE) as functions of current density at 20 °C under 1 bar and 10 bar CO_2 pressures. A total CO_2 feed flow rate of 20 sccm was maintained for both conditions.

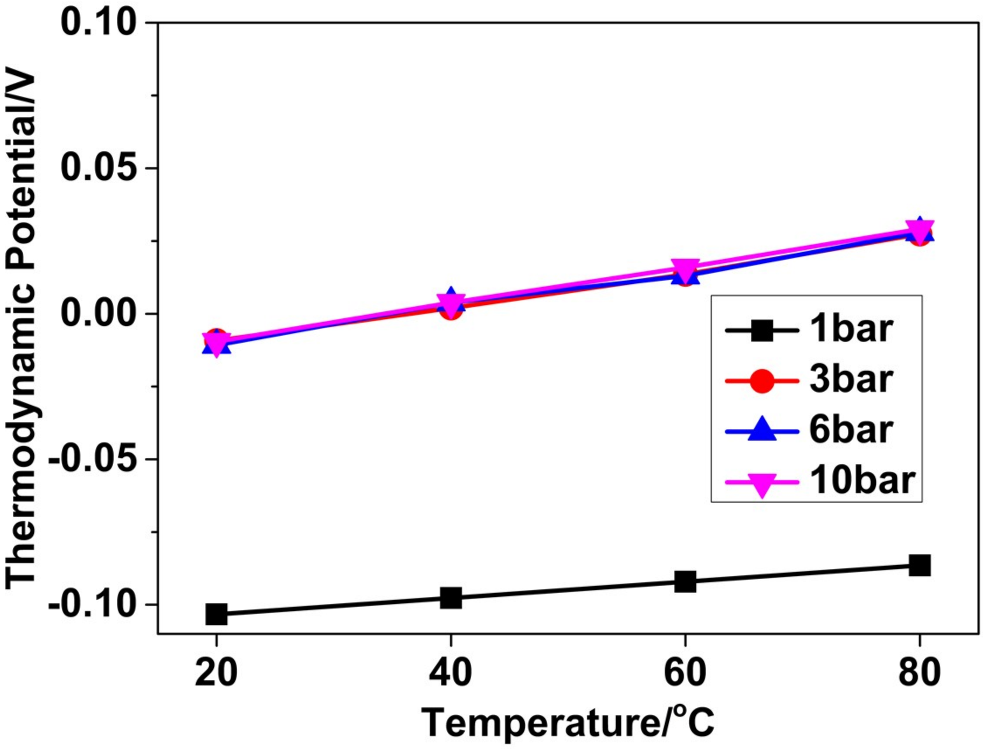

Figure S5. Calculated cathodic thermodynamic potential at various temperatures and pressure.

For the cathode reaction: $CO_2 + 2e^- + 2H^+ \rightarrow CO + H_2O$

The thermodynamic potential at different temperature was calculated using the following equation

$$E_r(T) = \frac{-\triangle G_r(T_{ref})}{nF} + \frac{\triangle S(T_{ref})}{nF}(T - T_{ref})$$

where $\triangle S_r$ was treated as constant from 20 °C to 80 °C.

The thermodynamic potential at different temperature was calculated using the following equation

$$E_r(T,P) = E_r(T) - \frac{RT}{nF} In(\frac{a_{CO}a_{H2O}}{a_{CO2}a_{H^+}^2})$$

$$a_i = \frac{P_i}{P^0} = \frac{y_i \times P}{P^0}$$

where a_{H2O} and a_{H+} was treated as constant, and the y_{CO} and y_{CO2} was calcultated from the GC peak area.

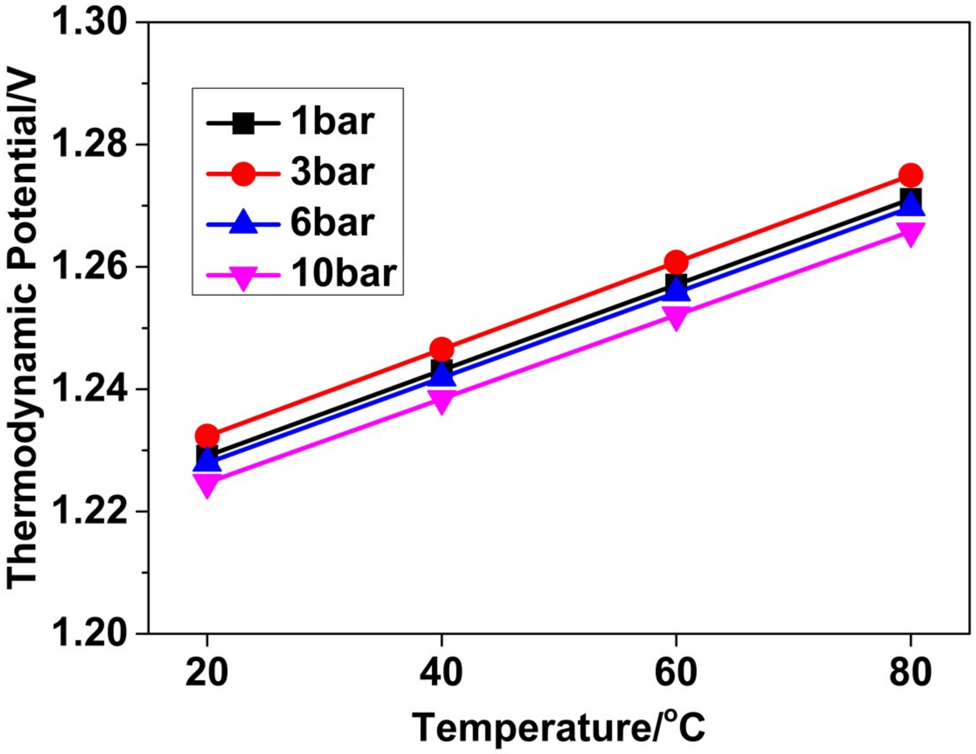

Figure S6. Calculated anodic thermodynamic potential at various temperatures and pressure.

For the anode reaction: $H_2O - 2e^- \rightarrow \frac{1}{2}O_2 + 2H^+$

The thermodynamic potential at different temperature was calculated using the following equation

$$E_r(T) = \frac{-\triangle G_r(T_{ref})}{nF} + \frac{\triangle S(T_{ref})}{nF}(T - T_{ref})$$

where $\triangle S_r$ was treated as constant from 20 °C to 80 °C.

The thermodynamic potential at different temperature was calculated using the following equation

$$E_r(T,P) = E_r(T) - \frac{RT}{nF} In(\frac{a_{o2}^{0.5} a_{H^+}^{2}}{a_{H2O}})$$

$$a_i = \frac{P_i}{P^0} = \frac{y_i \times P}{P^0}$$

where a_{H2O} and a_{H+} was treated as constant. For the anolyte, 0.1 M $KHCO_3$ was used, with the equilibrium reaction: $HCO_3^- + H^+ \rightarrow CO_2 + H_2O$, y_{O2} is assumed to be 0.2.

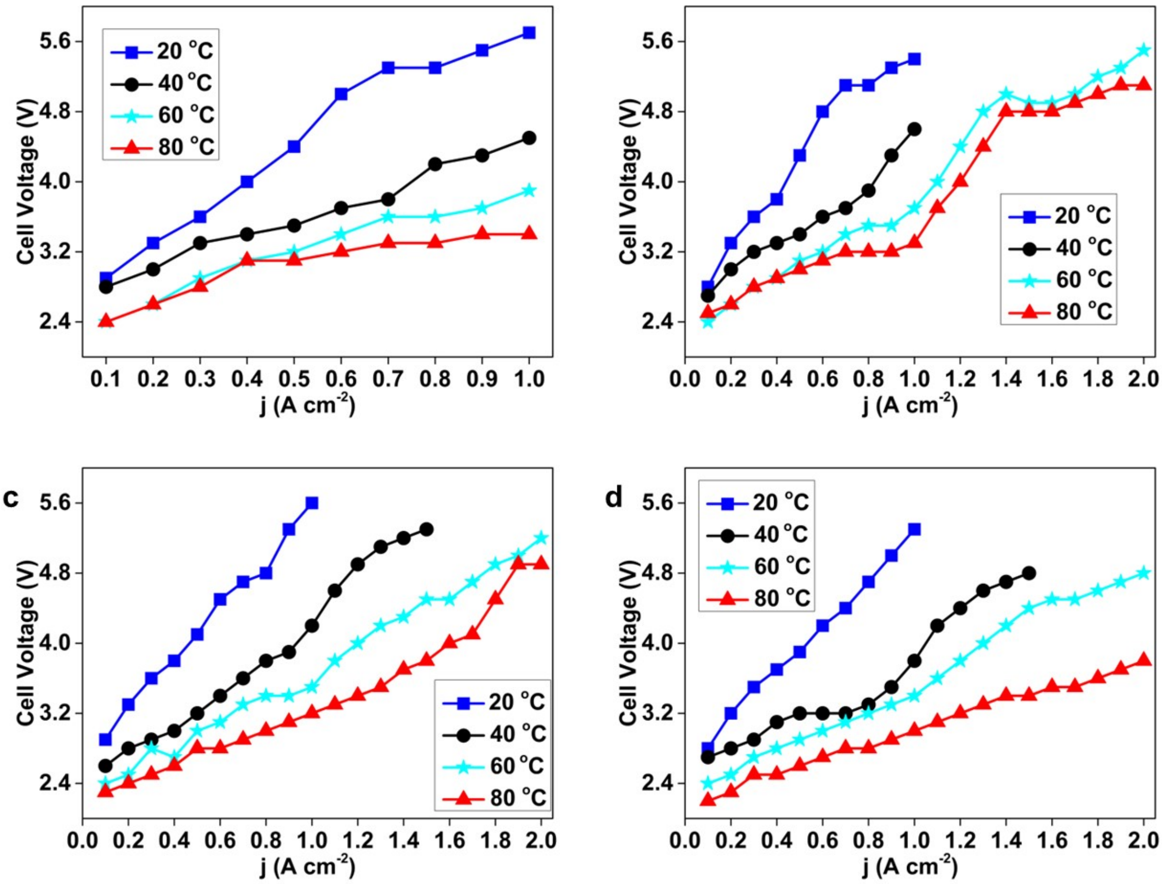

Figure S7. Temperature effect on CO_2RR cell voltage at (a)1 bar, (b)3 bar, (c) 6 bar, and (d)10 bar

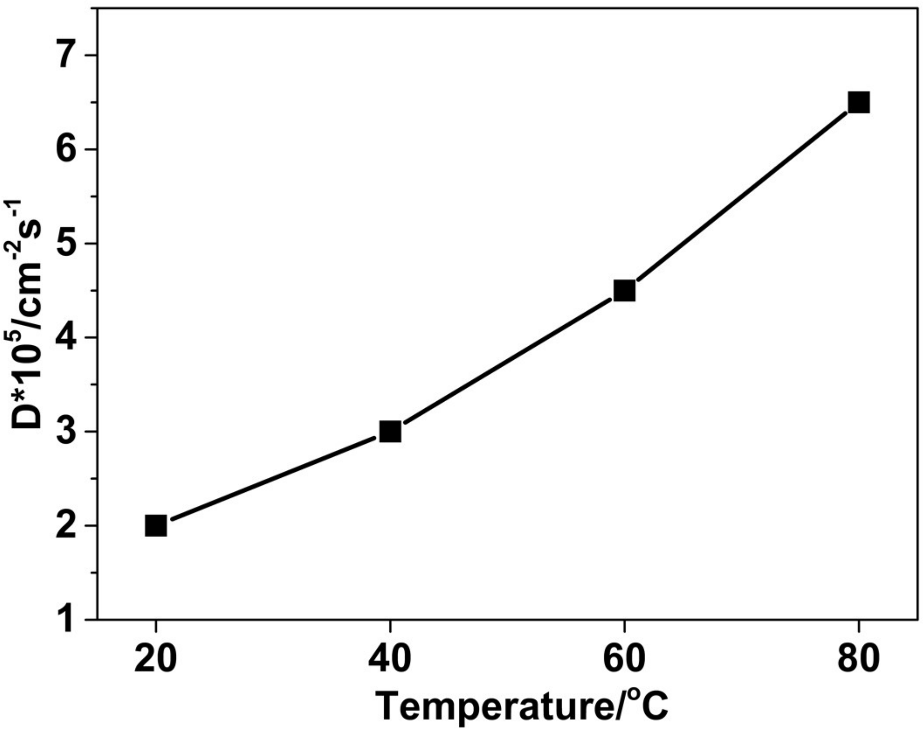

Figure S8. CO_2 diffusion coefficients (D) in water at various temperatures.[1]

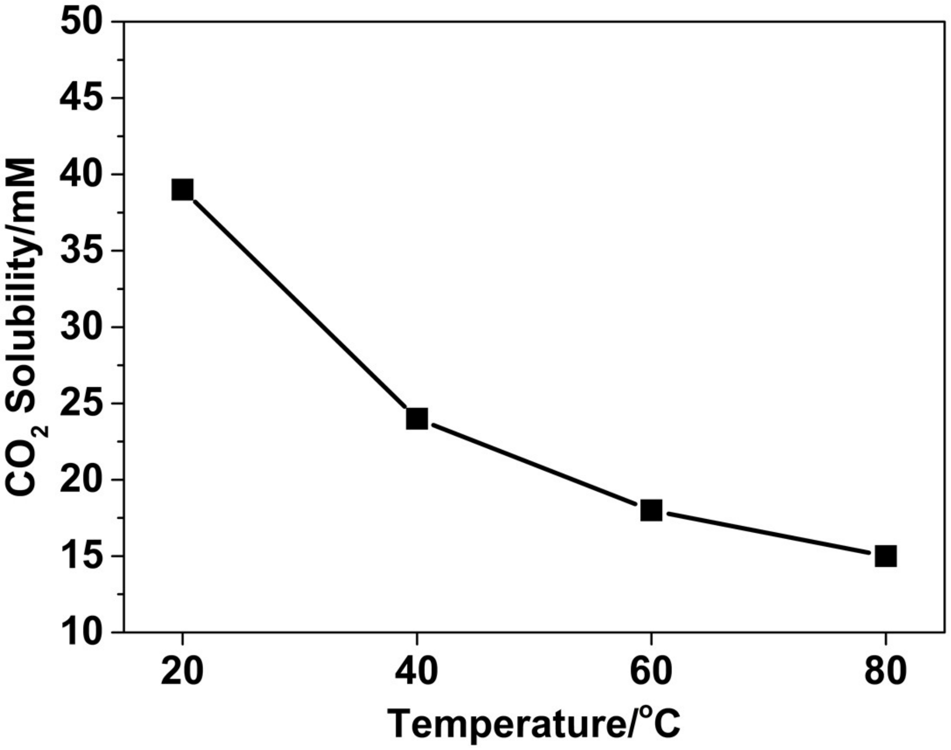

Figure S9. CO_2 solubility in water at 1 bar at various temperatures.[2]

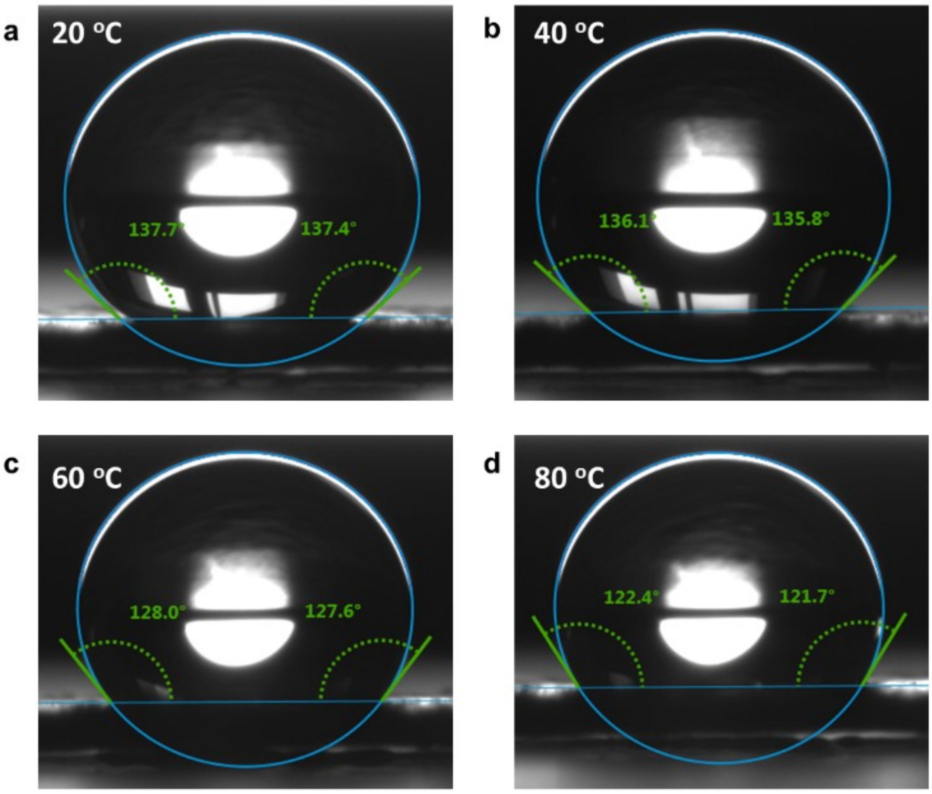

Figure S10. Contact angle measurements of water droplets on Ag GDEs at varying temperatures: (a) 20 °C, (b) 40 °C, (c) 60 °C, and (d) 80 °C.

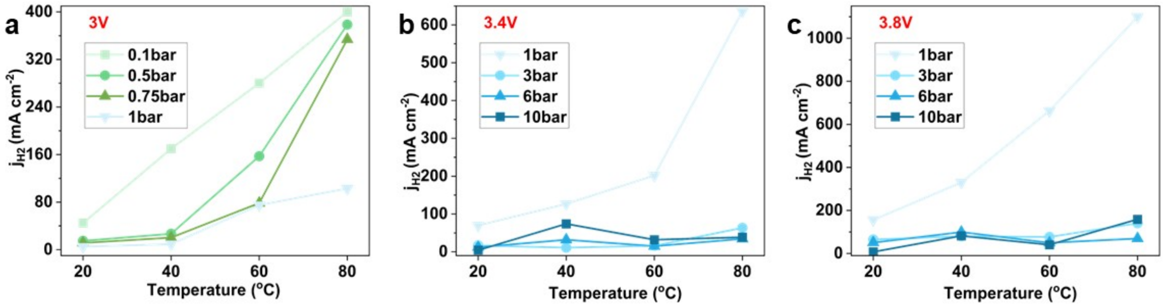

Figure S11. Effect of reaction temperature on the CO_2RR performance: j_{H2} as functions of temperature at various CO_2 partial pressures for applied cell voltages of (a) 3 V, (b) 3.4 V, and (c) 3.8 V. A total flow rate of 250 sccm was used for the CO_2RR at 3 V.

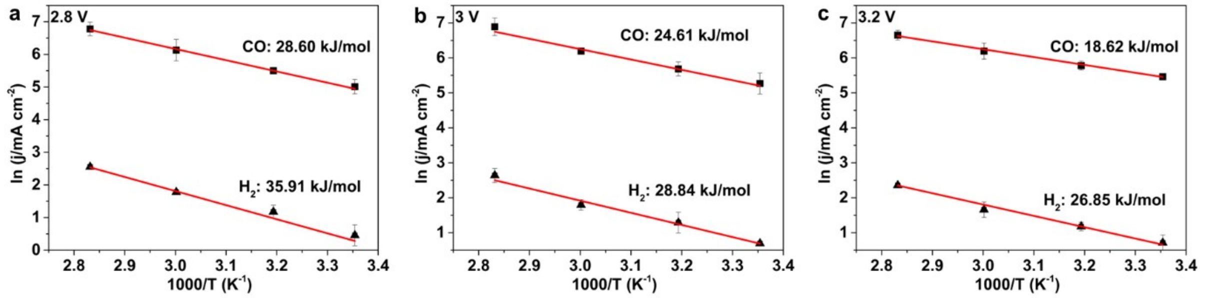

Figure S12. E_d for CO and H_2 under 10 bar at (a) 2.8 V, (b) 3 V and (c) 3.2 V. The error bars represent standard deviations of three independent measurements.

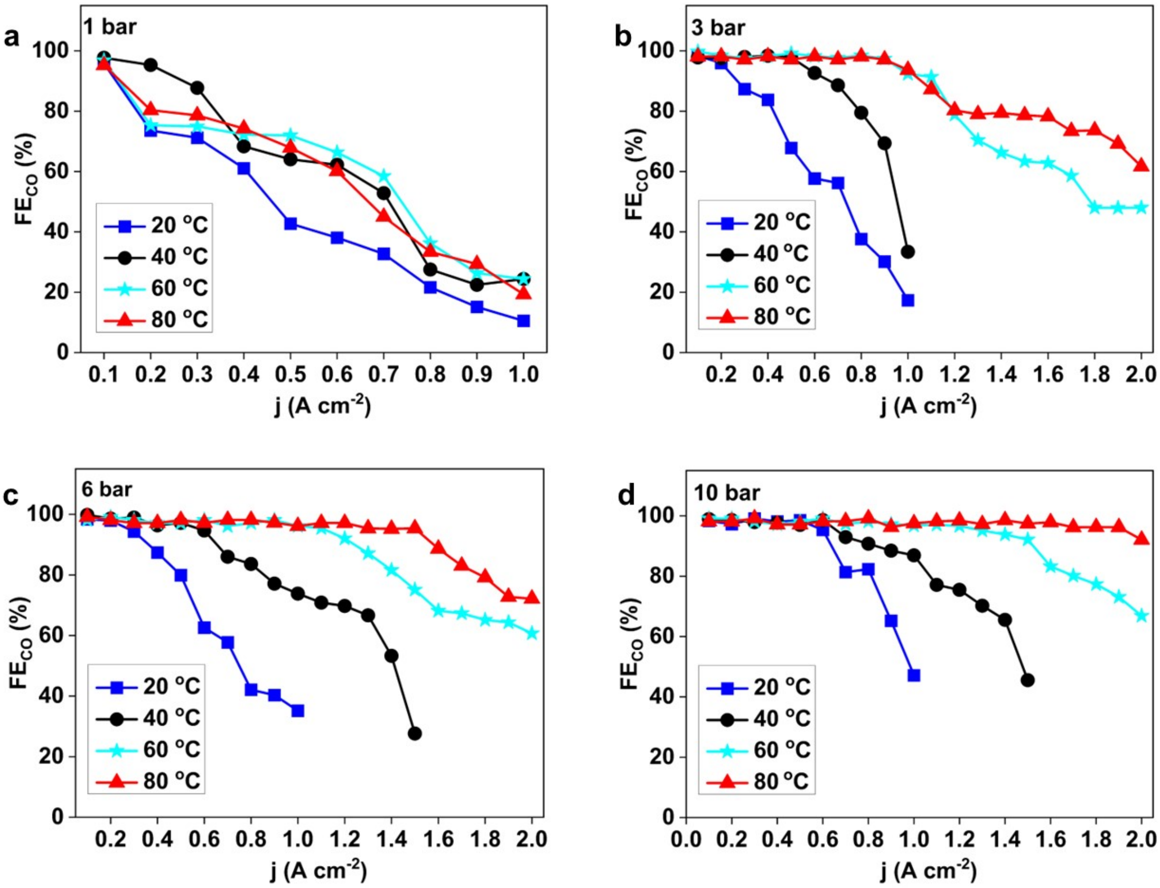

Figure S13. Temperature effect on FE$_{CO}$ at CO_2 pressure of (a)1 bar, (b) 3 bar, (c) 6 bar, and (d)10 bar.

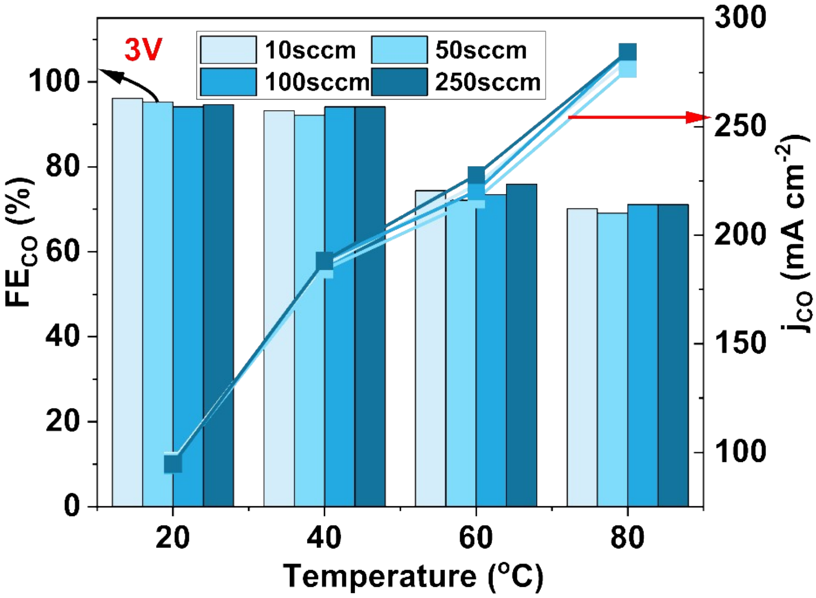

Figure S14. Temperature effect on FE_{CO} and j_{CO} under different CO_2 flow rates. The CO_2RR was conducted at 3 V with CO pressure of 1 bar.

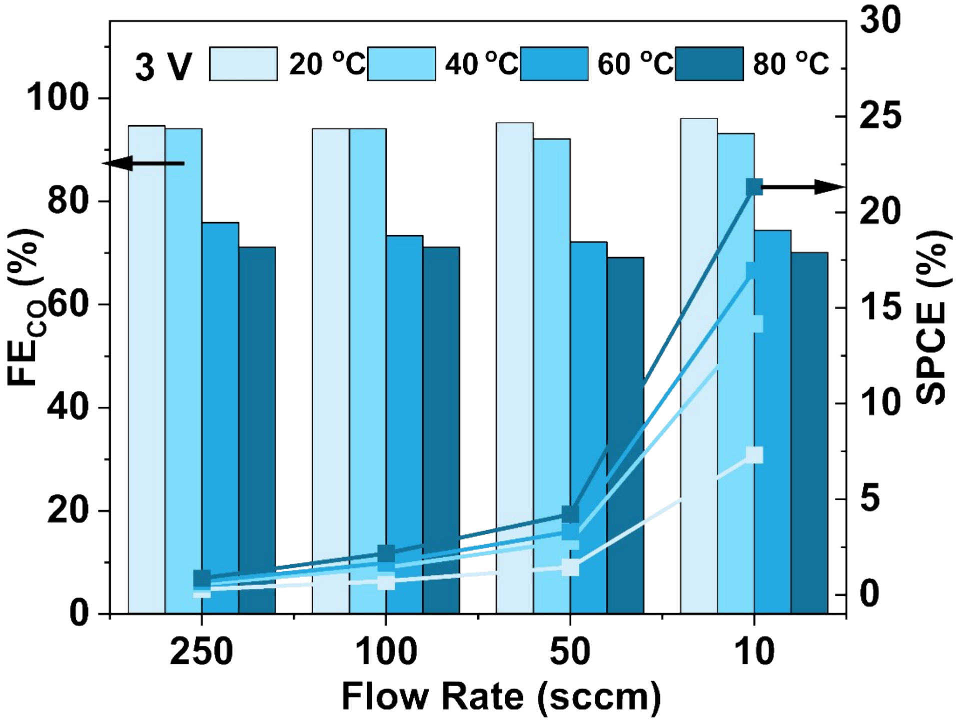

Figure S15. Temperature dependence of FE$_{CO}$ and SPCE under different CO_2 flow rates (10, 50, 100, and 250 sccm). The CO_2RR was conducted at 3 V under a CO_2 pressure of 1 bar.

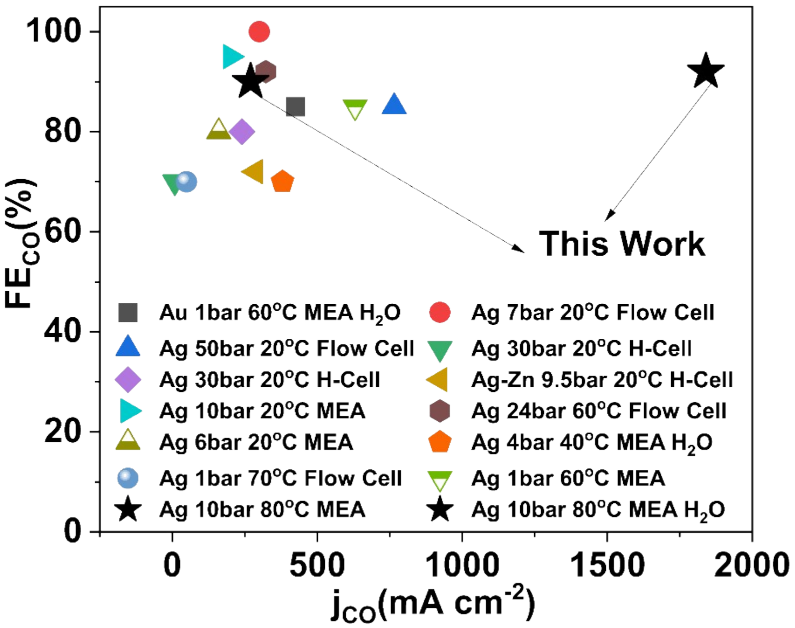

Figure S16. Comparison of CO_2RR performance on Ag-based catalysts under various reported conditions. The plot illustrates the relationship between FE_{CO} and j_{CO}. Data points represent different studies employing Ag and Au catalysts in various configurations, including H-cells, flow cells, and MEA systems, across a range of operating pressures and temperatures.[3-14]

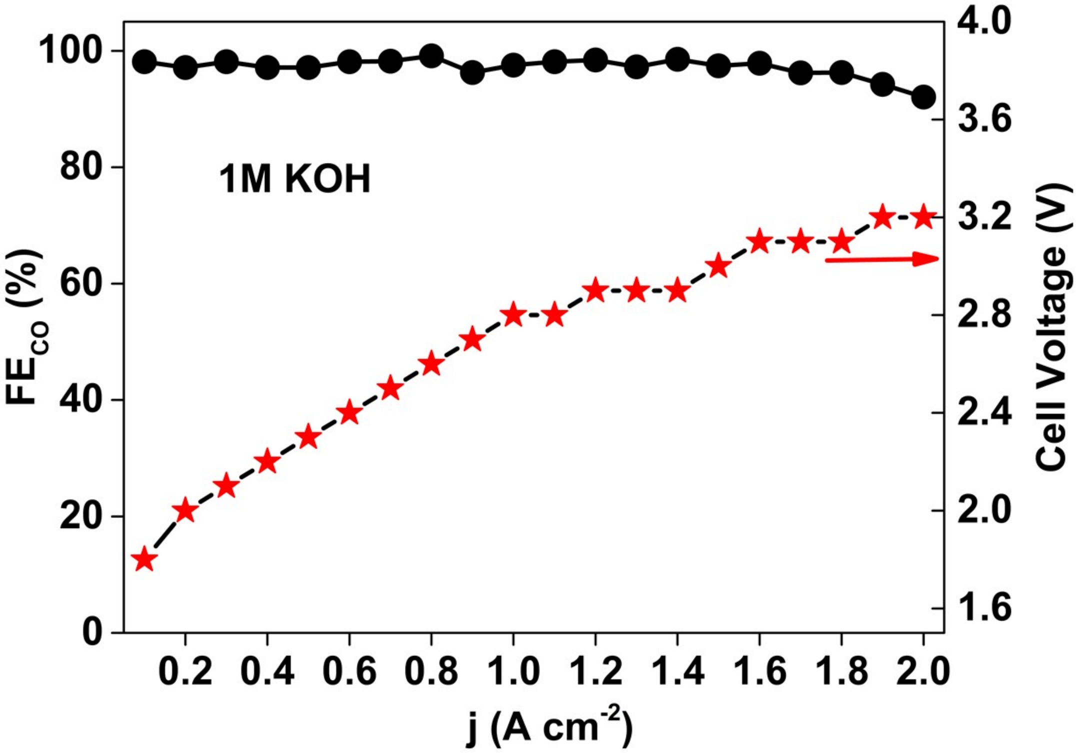

Figure S17. FE$_{CO}$ and cell voltage as a function of current density for CO_2RR in 1 M KOH anolyte at 80 °C and 10 bar.

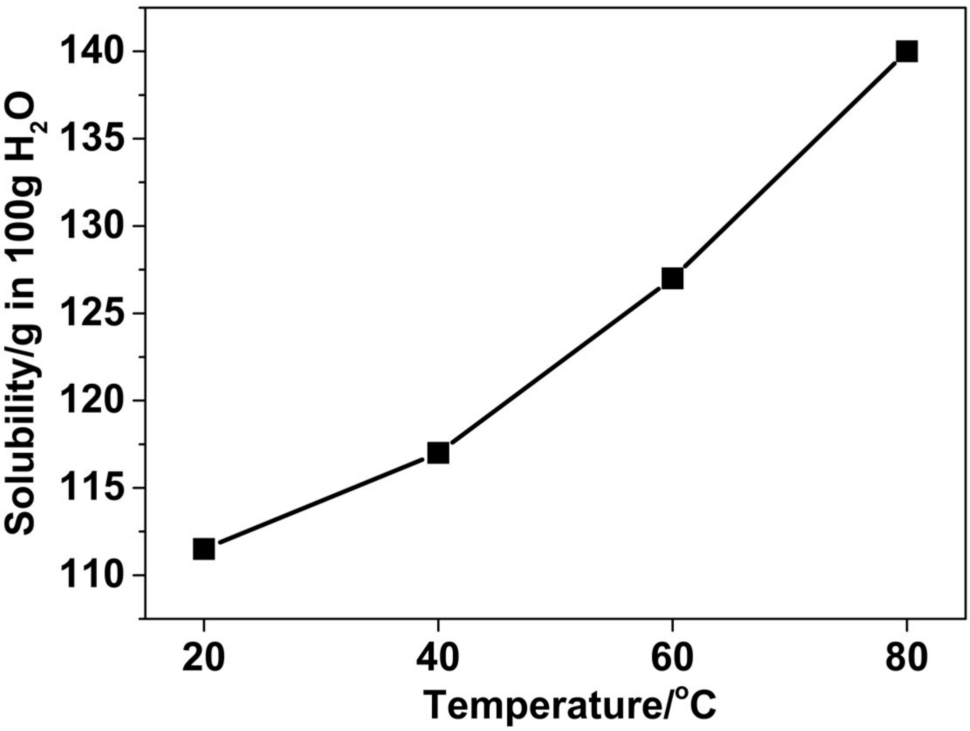

Figure S18. K_2CO_3 solubility in water at various temperatures.

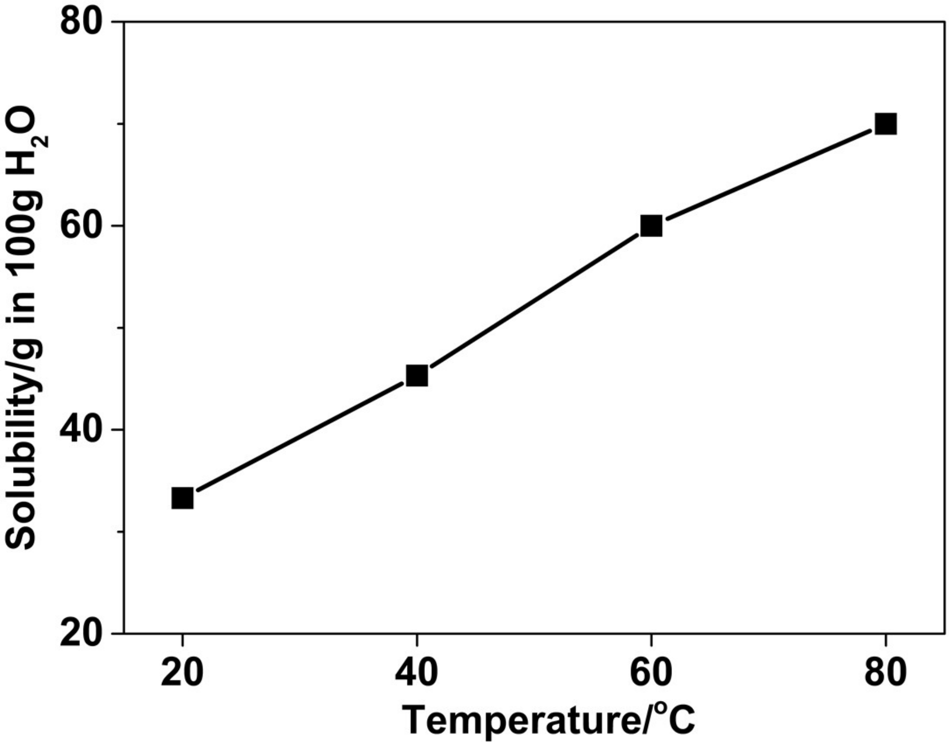

Figure S19. $KHCO_3$ solubility in water at various temperatures.

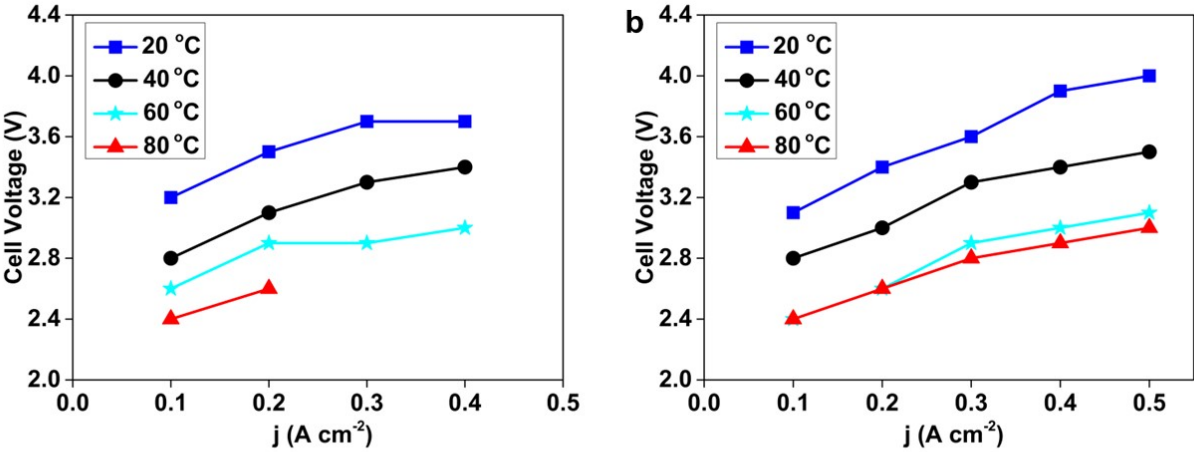

Figure S20. Temperature effect on cell voltage at (a)10 vol% CO_2, 1 bar and (b)10 vol% CO_2, 10 bar. 0.1M $KHCO_3$ was used as an anolyte.

Techno-economic analysis

Case 1: Comparison of pure CO_2 electrolysis under ambient and pressurized conditions

Table S1: Electrocatalytic performance under ambient and pressurized conditions using pure CO_2 feedstock.

Reaction parameter	20 °C, 1 bar	80 °C, 10 bar
Current density	100 mA cm^{-2}	900 mA cm^{-2}
Cell Voltage	2.9 V	2.9 V
FE_{CO}	95 %	96 %

As shown in **Table S1**, both systems exhibit comparable performance in terms of cell voltage (2.9 V) and FE_{CO} (~95–96%). However, the high-pressure system achieves a ninefold increase in current density (900 vs. 100 mA cm^{-2}), enabling significantly higher productivity. Based on previous TEA models[15], electrolyzer capital cost scales linearly with the required electrode area. Therefore, the high-pressure system requires only 11% of the electrolyzer cost compared to the ambient system for the same CO output.

To account for the additional hardware costs associated with pressurization—such as reinforced reactor housings, pressure-rated piping, and high-pressure flow pumps—we assume a one-time capital expense equivalent to 25% of the base electrolyzer cost, following estimates from prior high-pressure system assessments[16].

Factoring both benefits and added costs, the total system cost at 80 °C and 10 bar is estimated to be only 14% of that of the ambient pressure system, demonstrating the strong techno-economic potential of pressurized CO_2 electrolysis.

Case 2: Comparison of pure and diluted CO_2 electrolysis under ambient and pressurized conditions

Table S2: Electrocatalytic performance comparison between pure and 10% CO_2 feedstocks under ambient and pressurized conditions.

Reaction parameter	20 °C, 1 bar, 100% CO_2	20 °C, 10 bar, 10% CO_2
Current density	100 mA cm^{-2}	100 mA cm^{-2}
Cell Voltage	2.9 V	2.9 V
FE_{CO}	95 %	95 %

As shown in **Table S2**, both the ambient (20 °C, 1 bar, 100% CO_2) and pressurized (20 °C, 10 bar, 10% CO_2) systems demonstrate comparable electrochemical performance, with similar cell voltages (2.9 V) and FE_{CO} (~95%) at a current density of 100 mA cm^{-2}. This indicates that the electrolyzer capital cost remains unchanged across these conditions.

To evaluate the additional cost of gas pressurization, we consider a three-stage compression system, which has been shown to operate efficiently for low-pressure feed gases. Based on previous reports[17], the ideal work required to compress simulated flue gas from 1 bar to 10 bar is 207.41 kJ kg^{-1} (equivalent to 0.2 GJ ton^{-1}). Assuming a conservative mechanical efficiency of 90% and leveraging renewable electricity priced at US$0.03 kWh^{-1}, the corresponding operational energy cost was calculated to be approximately US$1.9 per ton of flue gas. Additionally, accounting explicitly for capital expenditures, including compressor installation as well as routine and extraordinary maintenance (US$0.4 per ton of gas), we estimate a total pressurization cost of around US$2.3 per ton of gas. For a flue gas mixture containing 10% CO_2 by volume, this translates to a pressurization cost of ~US$23 per ton of CO_2 equivalent.

References:

(1) Löwe, A.; Rieg, C.; Hierlemann, T.; Salas, N.; Kopljar, D.; Wagner, N.; Klemm, E. Influence of Temperature on the Performance of Gas Diffusion Electrodes in the CO_2 Reduction Reaction. *ChemElectroChem* **2019**, *6* (17), 4497–4506.

(2) Vos, R. E.; Smaak, J. P.; Koper, M. T. The Temperature Dependence of Electrochemical CO_2 Reduction on Ag and CuAg Alloys. *J. Catal.* **2024**, *436*, 115613.

(3) Yin, Z.; Peng, H.; Wei, X.; Zhou, H.; Gong, J.; Huai, M.; Xiao, L.; Wang, G.; Lu, J.; Zhuang, L. An Alkaline Polymer Electrolyte CO_2 Electrolyzer Operated with Pure Water. *Energy Environ. Sci.* **2019**, *12* (8), 2455–2462.

(4) Gabardo, C. M.; Seifitokaldani, A.; Edwards, J. P.; Dinh, C.; Burdyny, T.; Kibria, M. G.; O'Brien, C. P.; Sargent, E. H.; Sinton, D. Combined High Alkalinity and Pressurization Enable Efficient CO_2 Electroreduction to CO. *Energy Environ. Sci.* **2018**, *11* (9), 2531–2539.

(5) Edwards, J. P.; Xu, Y.; Gabardo, C. M.; Dinh, C. T.; Li, J.; Qi, Z.; Ozden, A.; Sargent, E. H.; Sinton, D. Efficient Electrocatalytic Conversion of Carbon Dioxide in a Low-Resistance Pressurized Alkaline Electrolyzer. *Appl. Energy* **2020**, *261*, 114.

(6) Proietto, F.; Berche, F.; Galia, A.; Scialdone, O. Electrochemical Conversion of Pressurized CO_2 at Simple Silver-Based Cathodes in Undivided Cells: Study of the Effect of Pressure and Other Operative Parameters. *J. Appl. Electrochem.* **2020**, *51* (2), 267–282.

(7) Hara, K.; Kudo, A.; Sakata, T. Electrochemical Reduction of Carbon Dioxide Under High Pressure on Various Electrodes in an Aqueous Electrolyte. J. Electroanal. Chem. 1995, 391, 141–147.

(8) Lamaison, S.; Wakerley, D.; Blanchard, J.; Montero, D.; Rousse, G.; Mercier, D.; Marcus, P.; Taverna, D.; Giaume, D.; Mougel, V.; Fontecave, M. High-Current-Density CO_2-to-CO Electroreduction on Ag-Alloyed Zn Dendrites at Elevated Pressure. *Joule* **2020**, *4*, 395–406.

(9) Endrődi, B.; Kecsenovity, E.; Samu, A.; Darvas, F.; Jones, R. V.; Török, V.; Danyi, A.; Janáky, C. Multilayer Electrolyzer Stack Converts Carbon Dioxide to Gas Products at High Pressure with High Efficiency. *ACS Energy Lett.* **2019**, *4* (7), 1770–1777.

(10) Dufek, E. J.; Lister, T. E.; Stone, S. G.; McIlwain, M. E. Operation of a Pressurized System for Continuous Reduction of CO_2. *J. Electrochem. Soc.* **2012**, *159* (9), F514–F517.

(11) Park, J.; Kim, E.; Kim, S.; Lim, C.; Kim, H.; Ko, Y.; Choi, J.; Oh, H.; Lee, W. H. Deriving an Efficient and Stable Microenvironment for a CO_2 MEA Electrolyzer by Reverse Osmosis. *ACS Energy Lett.* **2024**, *9* (7), 3342–3350.

(12) Heßelmann, M.; Lee, J. K.; Chae, S.; Tricker, A.; Keller, R. G.; Wessling, M.; Su, J.; Kushner, D.; Weber, A. Z.; Peng, X. Pure-Water-Fed Forward-Bias Bipolar Membrane CO_2 Electrolyzer. *ACS Appl. Mater. Interfaces* **2024**, *16* (19), 24649–24659.

(13) Dufek, E. J.; Lister, T. E.; McIlwain, M. E. Bench-Scale Electrochemical System for Generation of CO and Syn-Gas. *J. Appl. Electrochem.* **2011**, *41* (6), 623–631.

(14) Endrődi, B.; Kecsenovity, E.; Samu, A.; Halmágyi, T.; Rojas-Carbonell, S.; Wang, L.; Yan, Y.; Janáky, C. High Carbonate Ion Conductance of a Robust PiperION Membrane Allows Industrial Current Density and Conversion in a Zero-Gap Carbon Dioxide Electrolyzer Cell. *Energy Environ. Sci.* **2020**, *13* (11), 4098–4105.

(15) Shin, H.; Hansen, K. U.; Jiao, F. Techno-economic assessment of low-temperature

carbon dioxide electrolysis. *Nat. Sustain.* **2021**, *4* (10), 911–919.

(16) Jin, J.; Wicks, J.; Min, Q.; Li, J.; Hu, Y.; Ma, J.; Wang, Y.; Jiang, Z.; Xu, Y.; Lu, R.; Si, G.; Papangelakis, P.; Shakouri, M.; Xiao, Q.; Ou, P.; Wang, X.; Chen, Z.; Zhang, W.; Yu, K.; Song, J.; Jiang, X.; Qiu, P.; Lou, Y.; Wu, D.; Mao, Y.; Ozden, A.; Wang, C.; Xia, B. Y.; Hu, X.; Dravid, V. P.; Yiu, Y.-M.; Sham, T.-K.; Wang, Z.; Sinton, D.; Mai, L.; Pang, Y. Constrained C_2 adsorbate orientation enables CO-to-acetate electroreduction. *Nature* **2023**, *617* (7962), 724–729.

(17) Xu, Y.; Edwards, J. P.; Zhong, J.; O'Brien, C. P.; Gabardo, C. M.; McCallum, C.; Li, J.; Dinh, C.; Sargent, E. H.; Sinton, D. Oxygen-tolerant electroproduction of C_2 products from simulated flue gas. *Energy Environ. Sci.* **2020**, *13* (2), 554–561.